EOSL

Electro-Optics Systems Laboratory
Department of Electrical and Computer Engineering
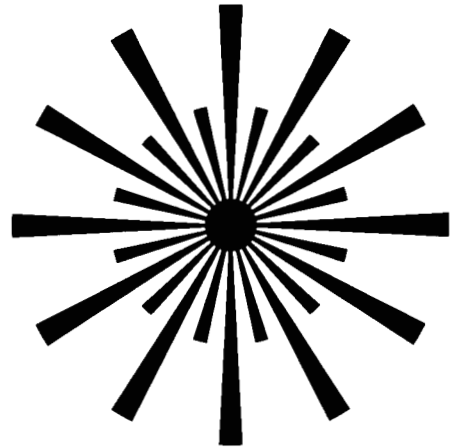
Evaluation of a Satellite Laser Ranging Technique Using Pseudonoise Code Modulated Laser Diodes

Carolyn Kay Ball
87-007 • December 1987

University of Illinois at Urbana-Champaign

EVALUATION OF A SATELLITE LASER RANGING TECHNIQUE USING PSEUDONOISE CODE MODULATED LASER DIODES

by

Carolyn Kay Ball

NATIONAL AERONAUTICS & SPACE ADMINISTRATION
Goddard Space Flight Center
Greenbelt, Maryland 20771

ELECTRO-OPTIC SYSTEMS LABORATORY
DEPARTMENT OF ELECTRICAL AND COMPUTER ENGINEERING
COLLEGE OF ENGINEERING
UNIVERSITY OF ILLINOIS
URBANA, ILLINOIS 61801

ABSTRACT

Several types of Satellite Laser Ranging systems presently exist, operating with pulsed, high-energy lasers. The distance between a ground point and an orbiting satellite can be determined to within a few centimeters. A new technique substitutes pseudonoise code modulated laser diodes, which are much more compact, reliable and less costly, for the lasers used now. Since laser diode technology is just achieving powerful enough lasers, the capabilities of the new technique are investigated.

Also examined are the effects of using an avalanche photodiode detector instead of a photomultiplier tube. The influence of noise terms (including background radiation, detector dark and thermal noise and speckle) that limit the system range and performance is evaluated.

TABLE OF CONTENTS

CHAPTER 1. INTRODUCTION

Since the mid-sixties, scientists and engineers have been using high-power lasers to range to earth orbiting satellites (including the moon). These large and often stationary systems measure the distance from their ground location to retroreflector-equipped satellites with accuracies of a few centimeters. Such accuracies allow for better measurements of tectonic plate motion, polar wobble, and variations in the Earth's rotation, to mention a few applications.

The design issues covered in laser ranging are very similar to basic laser communications techniques. Problems due to light modulation and detection, noise, and signal attenuation are common to both data communications and ranging. Ranging differs from typical laser-based data communications in its analysis of the error and its transmission media. Most data applications now use fiber, while ranging would require transmission through the atmosphere.

Early satellite laser ranging (SLR) techniques used pulsed Q-switched ruby lasers with pulse widths of a few tenths of a nanosecond. Most of the current systems use the more efficient mode-locked Nd:YAG lasers, operating typically at 5 pulses/s with 200 psec pulse widths. Pulse energies are normally 100 mJ [1].

An alternative to the pulsed ND:YAG techniques modulates laser diodes or laser diode arrays with a pseudonoise (PN) code. This method, described in detail in Chapter 2, has shown promise only in recent years with the development of high-power laser diode arrays (reports claim up to 2.5 Watts of continuous wave output power). Systems using arrays of laser diodes would be lighter, more rugged, and easier to operate and maintain than present systems while still operating with high accuracy and large range ambiguity. Comparisons of current options available in semiconductor lasers and arrays are made in Chapter 3.

This laser diode ranging technique is related to a previously established method of laser diode lidar (light detection and ranging) used for measuring aerosols [2]. Using a 30 mW laser diode, Takeuchi developed a lidar system with a range of a few kilometers. A random-modulation coding scheme was also used, operating with 60 nsec pulse widths.

A PN code is a sequence of on-off pulses which statistically resemble a random sequence. In this method, time-delayed versions of the transmitted code are correlated with the received signal (the transmitted code that has traveled to the target and back). The value of the time delay, τ_d, corresponding to the maximum correlation, is determined to be the optical propagation time. The distance to the satellite is related by

$$d = \frac{c\tau_d}{2} \ , \tag{1}$$

where c is the speed of light. The bit time of the PN code is also referred to as the chip time, T_c. The code period consists of M chips, and thus $T = MT_c$. The system resolution improves with smaller chip times (higher modulation frequency) as they are related by

$$\Delta z = \frac{cT_c}{2} \ . \tag{2}$$

The range ambiguity, that is, the maximum distance measuring capability, is restricted by the code period. If the time delay is longer than one code period, τ_d cannot be accurately determined, since more than one correlation would be maximized. Therefore, the maximum measurable range, z_a, is increased when the code period is increased,

$$z_a = \frac{cMT_c}{2} \ , \tag{3}$$

or, for a constant T_c, a larger M will increase z_a.

Another feature under investigation is the use of avalanche photodiodes (APDs) for detectors instead of photomultipliers. Silicon APDs are excellent detectors of the wavelengths emitted by laser diodes. In our system, however, the received signal is actually derived from counting individual photons; therefore, noise factors could dominate so weak a signal. APDs have several inherent noise factors whose contributions should be examined in this system: thermal noise, dark current noise, and noise due to the randomness of the gain. Although the APD gain can be optimized to reduce the noise factors, they must still be considered in the case of photon counting. A solution to the problem of thermal noise often used in other applications is to cool the APD to a low enough temperature so that its thermal noise will no longer overpower the signal. In Chapter 4, these factors are addressed in order to show that the noise does indeed limit the system.

Once the detector noise terms that cannot be neglected have been established, they are added to the evaluation of system error (Chapter 5). Since the optimum receiver for a PN code modulated system using ideal rectangular pulses is a correlation receiver, a search procedure can be used to determine the maximum likelihood estimate of the time delay. Ranging error cannot be totally eliminated from this system since the true time delay will actually lie somewhere within the interval that yields a peak correlation. An even larger ranging error will result if the detected signal is not strong and the noise creates other highly correlating intervals associated with incorrect time delays. The goal is to make this inherent error as small as possible. Computer simulations are used to confirm the theory, and help make potential system trade-offs easier to examine.

CHAPTER 2. RANGING SYSTEM DESCRIPTION

One of the most difficult things to do when describing a technical system is to clearly identify the many variables that define the system. This chapter is devoted to forming a clearer picture of the Satellite Laser Ranging System to be analyzed.

A diagram of a typical PN code modulated ranging system is shown in Figure 2.1. A PN code can be generated using a shift register, adders, and feedback connections. An N-stage shift register will yield a code of length $(2^N - 1)$ bits, or chips. The code will have 2^{N-1} ones and $(2^{N-1}-1)$ zeros in one period. These on-and-off bits, which are used to modulate the laser, also enter into a time delay sequence. The delayed versions are correlated with the noisy received signal, and a value is assigned to the time delay after a search for the peak correlations has been made.

A general point target detection system is illustrated in Figure 2.2. When the photodetection process assumes an ideal detector, the receiver is modeled as a correlation of the detected signal, s(t), and the delayed signal. Figure 2.3 is a block diagram of a possible implementation for this ranging receiver system. Assuming an ideal detector, narrow pulses are produced for each detected photocount of the received signal plus noise. These pulses are "anded" with delayed versions of the code. The outputs of the ands indicate when the detected and the delayed signals match, and the number of matches are counted over the integration period for each output. The value of the time delay that produces the largest count is the estimated range delay. Accuracy increases with shorter time-delay intervals and longer counting (integration) times.

In Figures 2.2 and 2.3, and throughout this analysis, a(t) represents the signal waveform. It may be shown in demonstration as on-off square pulses; however, a more realistic Gaussian form will be used in calculations, with

$$a(t) = e^{\frac{-t^2}{2\sigma_f^2}} , \tag{4}$$

where σ_f^2 is the Gaussian pulse variance. Therefore, as shown in Figure 2.4a, the PN code is represented using square pulses, and the code is obviously MT_c long. Part b of Figure 2.4 shows that after correlation, the peak of the correlations is the time delay. The continually repeating code thus causes the correlation function to also be periodic.

The receiver is known as a direct detection optical receiver because it responds to the instantaneous field intensity over the photodetector surface, and the detector output current is a point process. The photoelectron arrival times which create the current are modeled as a Poisson process.

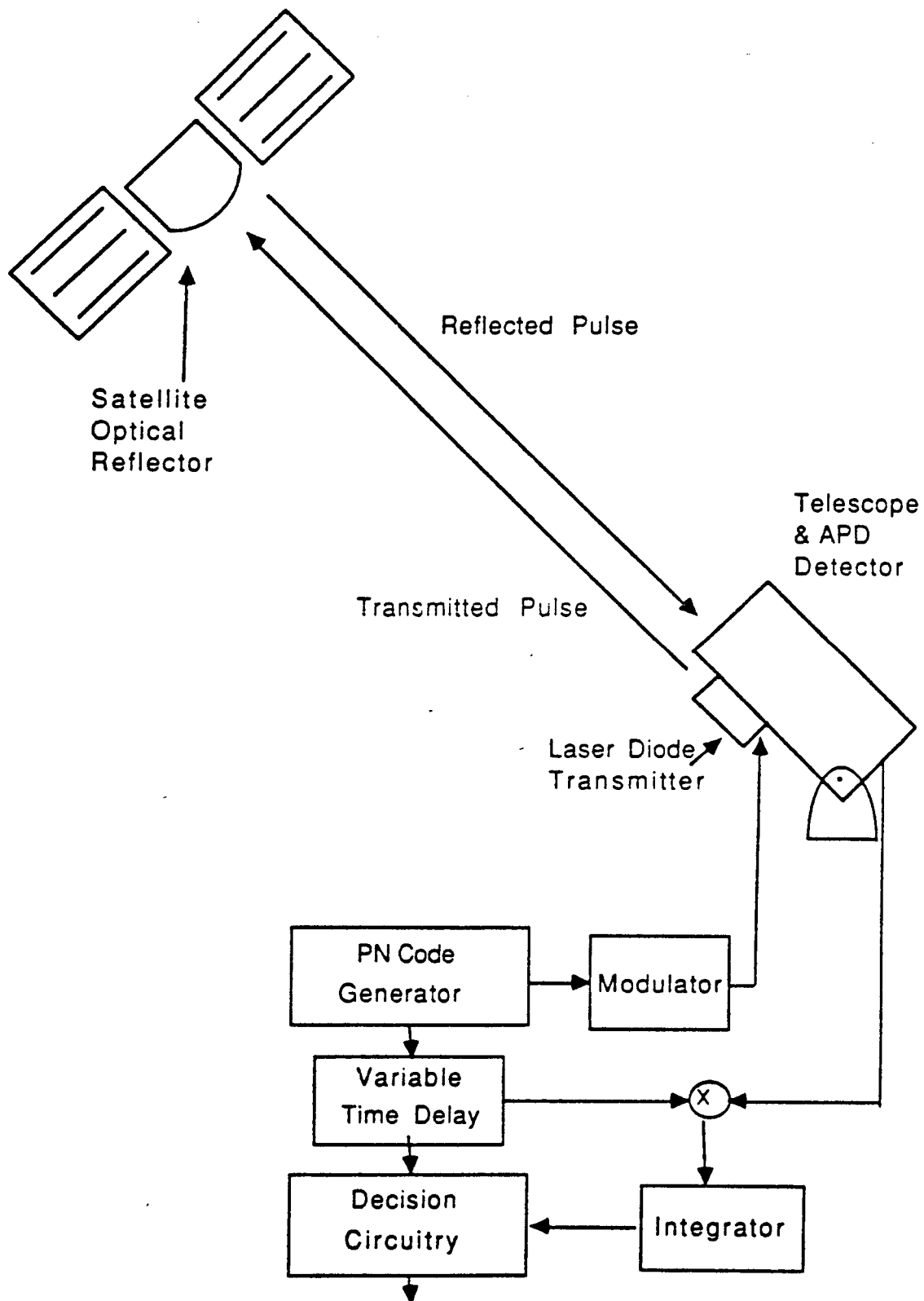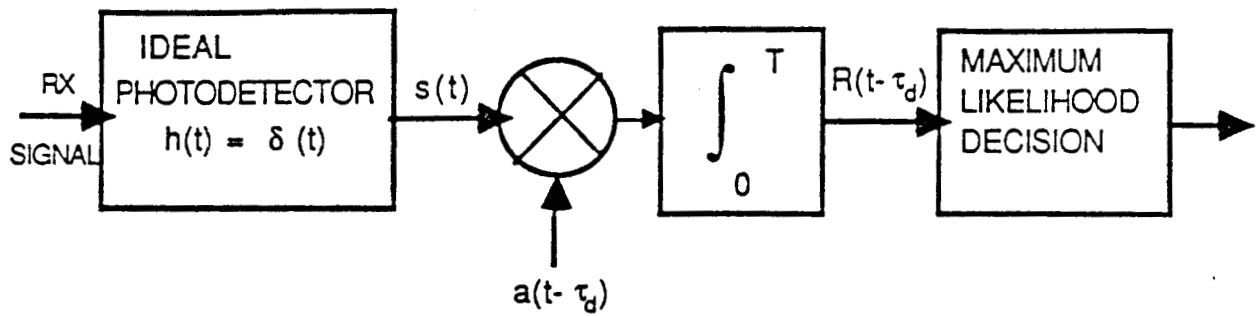Figure 2.1. Diagram of PN code Satellite Laser Ranging System.

4

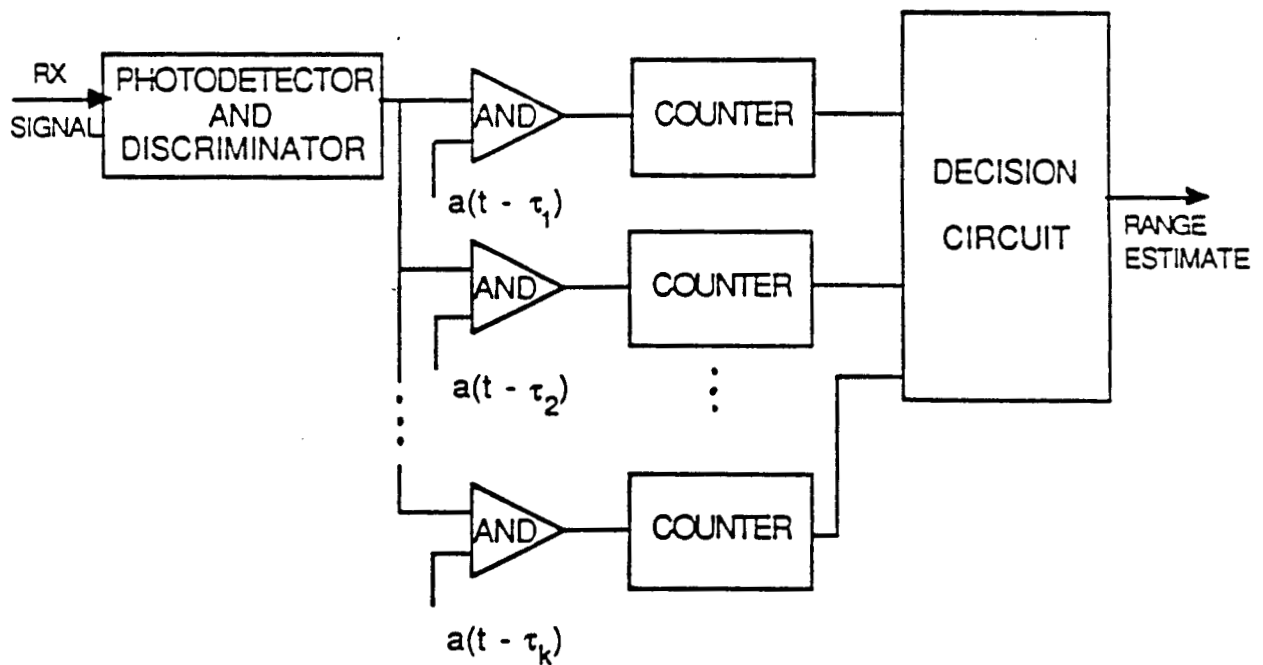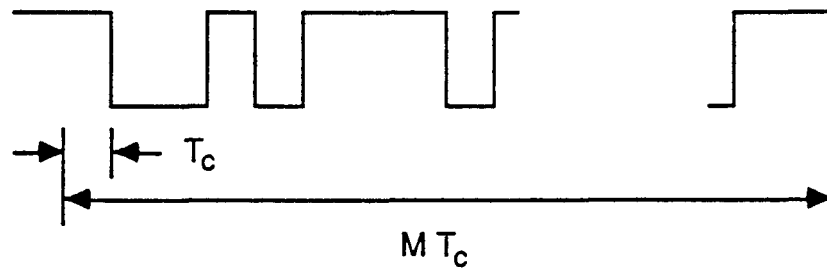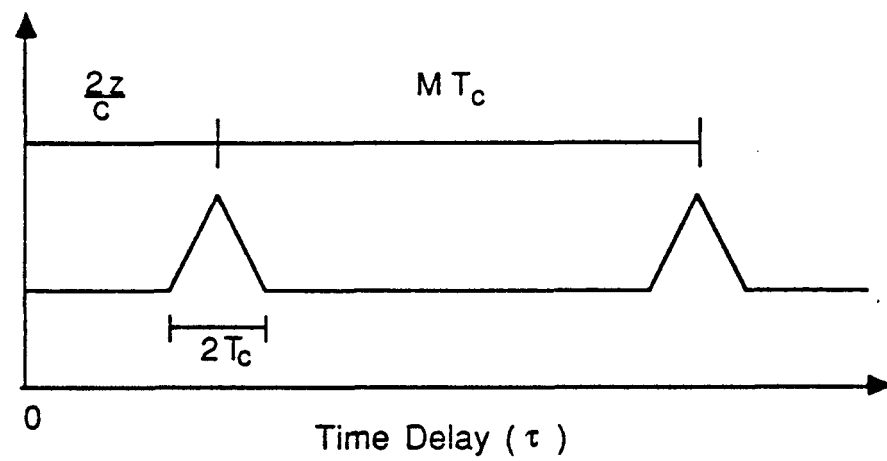Figure 2.2.   General ranging receiver.

Figure 2.3.   Block diagram of Receiving System.

5

a.

b.

Figure 2.4.   a. Transmitted PN code, b. Output from integrator (after correlation).

The noise processes also contribute to the current and are thus represented in the same way as photoelectron arrival rates. Photoelectron arrival rates will be designated in this analysis by λ with a subscript to signify the source. The mathematical conversion of instantaneous received intensity to arrival rate of photoelectrons detected at the receiver is

$$\lambda_R(t) = \frac{\eta \, P_R(t)}{h \nu} \, , \qquad (5)$$

where $P_R(t)$ is the total incident optical power, η is the detector quantum efficiency, and $h\nu$ is the energy of the photon [3]. On occasion, it may be advantageous to write expressions in terms of the average number of counts (or arrivals) per correlation period, which will be represented as $<N>_T$, where T is the correlation period.

Completing a description of this SLR system requires some comments on types of target models. Several satellites equipped with optical retroreflectors are orbiting the earth today. The primary target of most SLR systems, including the one described here, is the Laser Geodynamics Satellite (LAGEOS). LAGEOS, launched in 1976, was designed specifically to support a variety of scientific applications. Its cube-corner reflectors contribute to its 441 kgs, and it keeps a well-defined, stable orbit of 5900 km. LAGEOS serves as an inertial frame of reference which can be used to test ranging systems, thus it is the desired target model for this ranging method. The complexity of its mathematical model, however, requires that ranging to simpler targets first be established.

With this outline of the ranging system model, the next areas to be covered start with types of transmitters and detectors that are available for this SLR technique.

CHAPTER 3. SEMICONDUCTOR LASER TRANSMITTERS

Present satellite laser ranging transmitters operate in a pulsed mode, where the laser is off the majority of the time, letting the laser cool between pulses [4]. A PN code, however, requires near-continuous wave conditions (50% duty cycle operation) to produce the on-off chips of the continuous repeating code. The great losses that the signal encounters traveling to the target and back require that the average laser output be a least one watt. If the code has M chips and chip width T_c (usually less than one nsec), then each chip will have only a very small fraction of the average power. In comparison, present YAG laser-based techniques pack 100 mJ in each pulse at 5 pps. Thus in this technique, it is the detection process that must make up for the weaker signals, requiring less transmitter energy per pulse and making laser diodes a viable source.

3.1 Laser Diodes

Recent research in laser diodes, or semiconductor lasers, has lead to higher power devices because of improved methods of constructing the device's physical geometry and chemical composition, the foundation of its characteristics. Their basic structure consists of multiple layers of differently doped types of semiconductor material. A nondoped (or low-doped) region between n-type and p-type layers becomes the active region of the laser since it has a lower index of refraction than the n- and p-type regions. This tiny dielectric wave-guide allows light amplification between the crystal facets at each end of the diode.

Since nothing restricts the light from traveling laterally in the laser cavity, the beam emitted from this structure is elliptical, as can be seen in Figure 3.1. Two methods are used to limit the beam to a narrower lateral region, both using a change in the index of refraction outside the center of the active region to control the beam. Gain-guided lasers allow electrical contact only in a narrow longitudinal stripe, causing a local change in the index of refraction by injecting carriers (electrons and holes) in the areas just below it. The profile of injected carriers provides a weak complex wave-guide that confines the light laterally [4]. Figure 3.2 shows how index-guided lasers have lateral dielectric wave-confining structures, so that the active lasing region is formed by the real refractive index changes of the various materials. Index-guided lasers have typically had better (single-mode) far field beam patterns because they have better control of the lateral modes of the laser cavity. However, a new one-watt, single-element diode with a tapered-stripe, gain-guided structure was reported to have a "nearly single lobe" far field pattern [6]. This is the highest continuous-wave, single-element output reported to date.
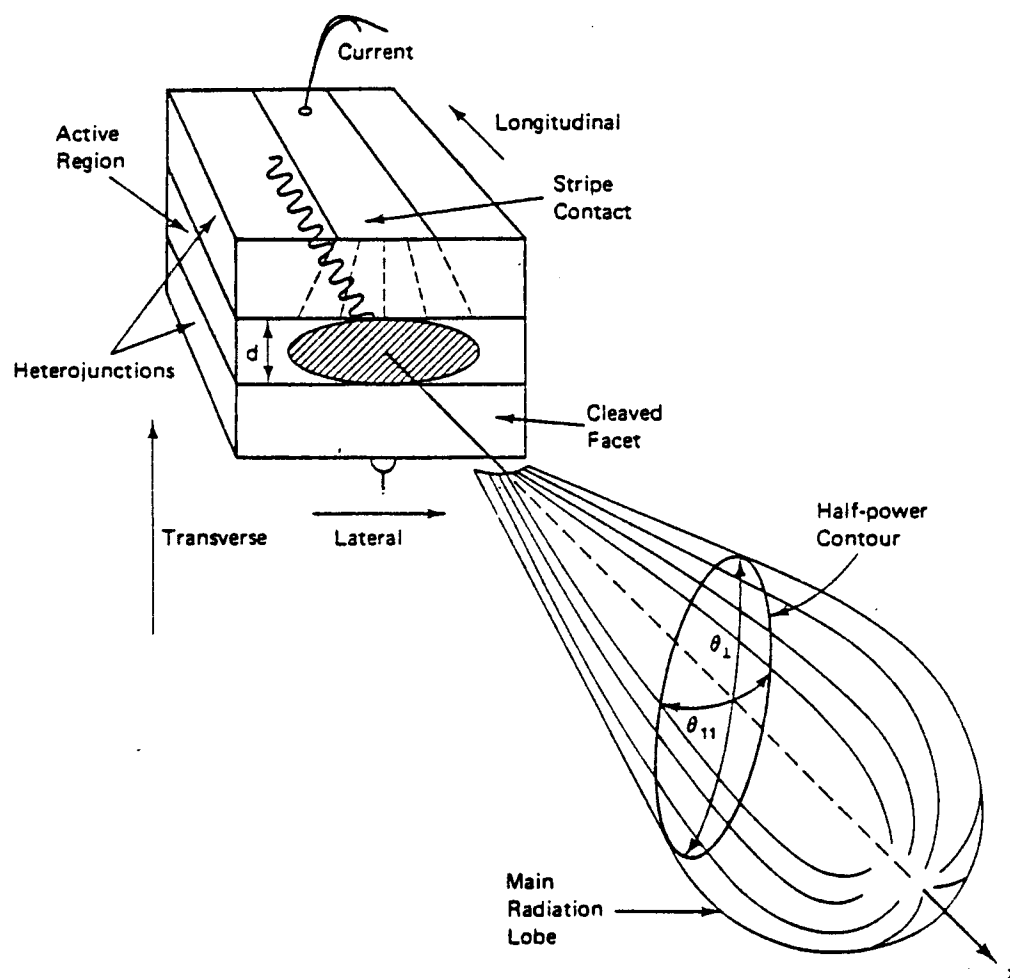
Figure 3.1. Diagram of a basic gain-guided laser diode illustrating elliptical output [5].
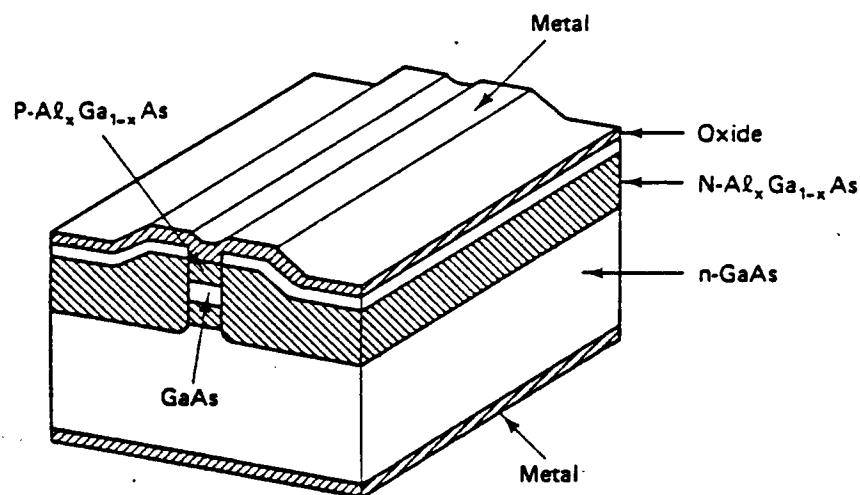
Figure 3.2. Example of an index-guided laser diode with a buried heterostructure geometry.

Until recently, continuous-wave power performance of a single diode was limited to much less than one watt. Light amplification in the laser cavity eventually increases enough to cause the destruction of its crystal facets. Antireflection coatings, nonabsorbing mirrors, and an increased lasing spot are some of the methods used to alleviate early catastrophic facet degradation by increasing the ratio of emitted power to internal lasing power. Silicon impurity induced disordering (IID) of the "window regions" is also becoming an attractive technique for the same purpose. Silicon impurities at the window facets increase that region's effective bandgap, therefore increasing the energy level that will cause catastrophic damage in that region.

Laser materials grown by metal organic vapor deposition (MOCVD) and molecular beam epitaxy (MBE) have also improved laser performance. These techniques are producing superior semiconductor crystals, drastically reducing material impurities. They have played the key role in making high-power laser diodes possible.

3.2 Laser Diode Arrays

Coupling a line of devices together to form a phase-locked array is another way to achieve high-power laser diode packages. Up to forty elements have been grown on the same substrate [7] to achieve a total high-power output. When powered through their common electrical contact, each element's optical modes propagate through their respective active regions and overlap a little with its nearest neighbors. The sum of the single elements' modes is the overall mode of the device and is called the supermode. This dominating mode does not usually yield the preferred single-lobed, far-field beam pattern, especially when gain-guided arrays are used. Techniques are being developed to stabilize and smooth the beam pattern, decreasing the beam divergence. For application to Satellite Laser Ranging, a single-lobe pattern is optimum, but an imperfect, near-Gaussian pattern would be acceptable. Examples of currently available continuous-wave laser diodes and arrays are given in Table 3.1. The diodes listed here are in the 800 nm wavelength region and range in cost from $200 to $8000. The divergence angle given is without collimation. Several arrays are still in the experimental stage, not yet released commercially, as their lifetimes have not yet been established to reasonable levels.

Beam divergence and the extinction ratio due to continuous wave operation are two sources of error that are characteristic of both laser diodes and arrays. In order to turn the laser on quickly enough, it must be biased just at threshold, so it actually never shuts completely off, transmitting a small amount of energy during a zero. The ratio of energy transmitted during an "on" pulse to that of an "off" pulse is called the extinction ratio, and it must be considered when analyzing the system's performance. This phenomenon will be addressed in Chapter 5. The beam divergence should be as small as possible so that the energy will not spread excessively during propagation.

10

This parameter becomes a factor in determining the amount of energy that can be expected to be returned to the receiver. A collimating lens can greatly reduce the divergence. Signal reduction due to beam divergence is accounted for in the calculation of the received signal count rate.

The state-of-the-art is just now reaching the necessary power requirements of our laser ranging techniques while maintaining good beam quality and reliability. Both laser diodes and laser diode arrays are now obvious choices for laser transmitters where simplicity, ruggedness, lifetime and cost are important.

Table 3.1

High-Power Cw Laser Diodes

Manufacturer	Model	Number of Elements	Output Power (W)	Divergence Angle *
Sony	SLD304V	1	1.0	11° x 35°
Sharp	LTO90	1	0.10	11° x 33°
M/A Com.	LCW-10	1	0.01	12° x 35°
Spectra Diode Labs	SDL-2460	20	1.0	10° x 40°
Spectra Diode Labs	(experimental)	10	2.1	19° x 34°
Spectra Diode Labs	(experimental)	40	2.6	--

*uncollimated

CHAPTER 4. DETECTION SYSTEMS

4.1 Comparison of Detection Techniques

Present Satellite Laser Ranging (SLR) detection systems typically use either the conventional dynode-chain photomultipliers or the newer microchannel-plate (MCP) photomultipliers (PMTs). Both offer high gains (around 10^6), but MCP PMTs offer shorter transit times (electron propagation time) and smaller jitter (variations in transit time). Although MCP PMTs may have a quicker response, an avalanche in a channel depletes it of charge for several microseconds, adding to the dead time [8]. Since these direct detection systems operate under pulsed conditions, they can absorb the delay time. But the SLR technique proposed is continuously modulated at more than 1 GHz, making even the shorter PMT dead times of a few nanoseconds too slow. However, multiple correlations of the continuously repeated PN code reduce the gain requirement, and now another type of detector becomes a contender: the avalanche photodiode.

Photodiodes are more rugged, have longer lifetimes and higher quantum efficiencies, and can be modulated faster than photomultipliers. P-I-N photodiodes do not have enough gain for low-level applications, but avalanche photodiodes (APDs) operated normally, or in "Geiger mode" can be used for photon counting. PMTs typically have a quantum efficiency of 10%-15%, where APDs can have quantum efficiencies as high as 85%. At best, PMTs have a dead time of about 2 nsec. Although an APD's capacitance generally limits its modulation capability to about 1 GHz, up to 8 Gb/sec has been achieved in special circuit designs that sacrifice some gain [9]. These characteristics indicate that APDs may now be favored over photomultipliers in SLR systems.

4.2 Detector Noise

Direct detection systems encounter several types of noise as the incident photons ionize to produce electrons: background noise, dark current produced in the device from random diffusion and recombination, gain fluctuations (for gains greater than one) due to the randomness of multiplications for each event, thermal noise from the device, and shot noise related to the signal power. Thermal noise often dominates the other noise contributors unless the signal is very strong, then shot noise may dominate. However, for the case of photon counting (i.e., a weak signal), all noise terms must be considered.

Since the detector cannot discriminate between the signal input and input from other light sources, the contribution to the output current from other input sources adds to the system noise.

12

Filters can reduce the optical bandwidth of the receiver so that only background radiation at the same wavelength as the signal will be seen at the detector input. This background noise is added to the signal to become the total power detected, and is accounted for in the shot noise term. The total arrival rate (from Eq. 5) can also be expressed as

$$\lambda_R(t) = \lambda_s \, a(t) + \lambda_b \quad , \tag{6}$$

where a(t) is the signal waveform (ideally on/off square pulses, but calculated as described in Eq. (4)), λ_s is the continuous signal arrival rate and λ_b is the constant background arrival rate.

Dark current is the photodiode current present when there is no incident optical radiation. It is inherent to the device structure, and consists of two components [10]. Usually called the bulk current, this output is due to carriers generated in or diffused into the depletion layer of the photodiode. This component is subject to gain in the device, just at the input signal is. The other component is due to surface currents set up under the action of the bias field, and does not undergo multiplication. Since impurities are the cause of these stray currents, improving the material quality directly reduces them. Ionization rates are also affected by temperature, so lowering the device temperature also reduces the spontaneous ionizations that make the dark current. Some structural designs also reduce carrier regeneration in the depletion region since its current is related to the region's area, width, and intrinsic carrier concentration.

Avalanche photodiodes can be biased for a mean gain, but the avalanche mechanism is actually a varying random process. Theoretical expressions for the true, non-Gaussian distributions of the gain have been established by McIntyre [11] and Conradi [12] since 1972; however, they are quite complicated. The noise due to gain fluctuations, called the excess noise factor, is defined as

$$F = \frac{<G^2>}{<G>^2} \quad , \tag{7}$$

and is determined using a gain-dependent model [13]

$$F(G) = (2 - \frac{1}{G})(1 - k_{eff}) + k_{eff} \, G \quad , \tag{8}$$

where k_{eff} is the electron ionization coefficient ($k_{eff} = 0.2$ for silicon).

Thermal fluctuations of electrons in a resistor cause thermal (or Johnson) noise in any electronic system. Assuming $R_{Load} >> R_{Internal}$, the load resistor is given the blame for thermal fluctuations in the RC-modeled APD detection circuit. Since the thermal noise is independent of frequency, it can be treated as white noise. Using the RC filter representation, and assuming the detector bandwidth is greater than the two-sided modulation bandwidth for good output pulse

13

distribution, the thermal noise autocorrelation function in current units is [14]

$$R_{th}(\tau) = \frac{2 k_B T^o}{R_L} \delta(\tau) \quad , \tag{9}$$

at the filter input, and is

$$R_{th}(\tau) = \frac{2 k_B T^o B}{R_L} e^{-|\tau|/R_L C} \quad , \tag{10}$$

at the filter output. Since the variance of a zero-mean, wide-sense stationary process is equal to its autocorrelation function at $t = 0$, then,

$$\sigma_{th}^2 = \frac{2 k_B T^o B}{R_L} . \tag{11}$$

A Gaussian filter model is also a useful representation. Because thermal noise is treated as white noise, the noise output of any linear filter with an autocorrelation function $R_h(\tau)$ can be written as

$$R_{th}(\tau) = \frac{2 k_B T^o}{R_L} R_h(\tau) . \tag{12}$$

The statistical nature of the photon-to-electron conversion process causes random variations in the true value of the output current, called detector shot noise. Shot noise spectral density is also independent of frequency, so it, too, can be modeled as white noise. Since it is a function of the input power level, the strength of the noise depends on the strength of the input. The contribution of shot noise to the overall noise of the detection system can be found by first writing the signal current response as [14]

$$s(t) = \sum_{j=1}^{N_T(t)} e \, G_j \, h(t-\tau_j) + \sum_{j=1}^{N_L(t)} e \, h(t-\pi_j) \quad , \tag{13}$$

(ignoring thermal noise for a moment), where

$N_T(t)$ = the total number of counts generated in the interval $(-\infty, t)$ due to signal, background, and bulk dark current ,

$N_L(t)$ = the number of counts generated in the interval $(-\infty, t)$ due to surface leakage,

τ_j , π_j = sets of Poisson points that are the event "arrival times,"

$h(t)$ = the detector impulse response,

G_j = the gain for that particular event.

14

for arrival rates that are independent of the gain. This combines momentarily some of the noise terms with the received signal in order to simplify the expressions. Applying Campbell's theorem to Eq. (13), the mean and the variance of a signal are determined to be [15]

$$<s(t)> = e<G>\lambda_T(t) * h(t) + e\lambda_L(t) * h(t) , \qquad (14)$$

and

$$\sigma_s^2 = e^2<G^2>\lambda_T(t) * h^2(t) + e^2\lambda_L(t) * h^2(t) , \qquad (15)$$

where $\lambda(t)$ is the arrival rate associated with the corresponding $N(t)$. The contribution of the detected signal and background in the first term on the right-hand side of Eq. (15) is due to shot noise.

4.3 APD Performance in Normal Mode

Under normal operation, calculating a device's signal-to-noise ratio at its output is one measure of its performance. The definition of SNR is

$$SNR = \frac{\text{total signal power from signal photocurrent}}{\text{shot, background, dark current, and thermal noise power}} .$$

Thus, with the above noise terms, and using λ_R as defined in Eqs. (5) and (6), the SNR of an APD would be

$$SNR = \frac{[e<G>\lambda_R a(t)*h(t)]^2}{e^2 F<G^2>\lambda_T(t)*h^2(t) + e^2\lambda_L(t)*h^2(t) + \sigma_{th}^2} . \qquad (16)$$

Since the SNR is a function of the gain, to optimize the device it is necessary to take the derivative of the SNR with respect to the gain, G, and set it equal to zero. Solving this yields

$$G_{opt} = \left(\frac{2\left(\lambda_L(t) + \frac{2k_B T^o}{e^2 R_L}\right)}{k_{eff} \lambda_T(t)} \right)^{\frac{1}{3}} , \qquad (17)$$

where $F \approx 2.0 + keff\, G$. It should be noted that reliable APDs are limited to a gain of less than or about 250.

where $F \approx 2.0 + keff\ G$. It should be noted that reliable APDs are limited to a gain of less than or about 250.

Another concern of APDs in normal operation is the device bandwidth. To avoid having smeared output pulses, it is necessary that the device bandwidth (1/RC) be greater than the modulation bandwidth, B. This means that 1/RC >> B. Load resistance is typically about 200 ohms, so device capacitance must be kept as low as possible (less than a few picofarads).

4.4 Geiger Mode Operation

Another method of photon counting that has recently gained attention is "Geiger mode," or photon counting mode, operation of avalanche photodiodes. In this mode, the single photon avalanche diode, or SPAD, is biased above its breakdown voltage where a single photoelectron may trigger a self-sustaining avalanche. The avalanche current generated is large enough that no other amplification is needed. The only drawback to this method is that some type of "quenching " is needed to stop the avalanche and prepare the circuit to receive another photon. This results in a rather long delay time, usually on the order of a few hundred nanoseconds.

Resolution in geiger mode operations is approaching tens of picoseconds, which is more than adequate for PN code detection. A simplified active quenching circuit is shown in Figure 4.1. The dead time is approximately equal to twice the delay in the feedback loop since the avalanche current pulse is the width of this delay, and an equivalent negative pulse is used to quench the avalanche, preparing it for the next photon. A 30 nsec delay was reported for this circuit. It appears that the delay could be reduced by using a faster circuit design; however, it is necessary for the APD in this mode to remain disconnected for some time after an avalanche to prevent afterpulsing. Afterpulsing is caused by an electron liberated from some impurity site it had become trapped in during a legitimate avalanche, which then causes a new false avalanche. The probability of an afterpulse decreases with time, making a long dead time desirable. Gating the detection system might reduce some of the effects of afterpulses, but would not be very practical for continuous SLR detection. Better material with fewer impurities would also of course reduce this problem.

Therefore, although geiger mode operation is an attractive single photon counting technique, its deadtime and complexity may not make it the best choice for Satellite Laser Ranging applications using continuous modulation.

Although current research of APDs is not as dynamic as the research of laser diodes,ways of reducing the noise factors and increasing the modulation capability are still under investigation. Table 4.1 lists a few of the commercially available APDs. The capacitance is listed since it is an indicator of the maximum modulation bandwidth, related, as mentioned earlier, by B = 1/RC. RCA's model C30902 is often used experimentally in the literature and appears to offer the highest responsivity as well as shortest rise-time.

16
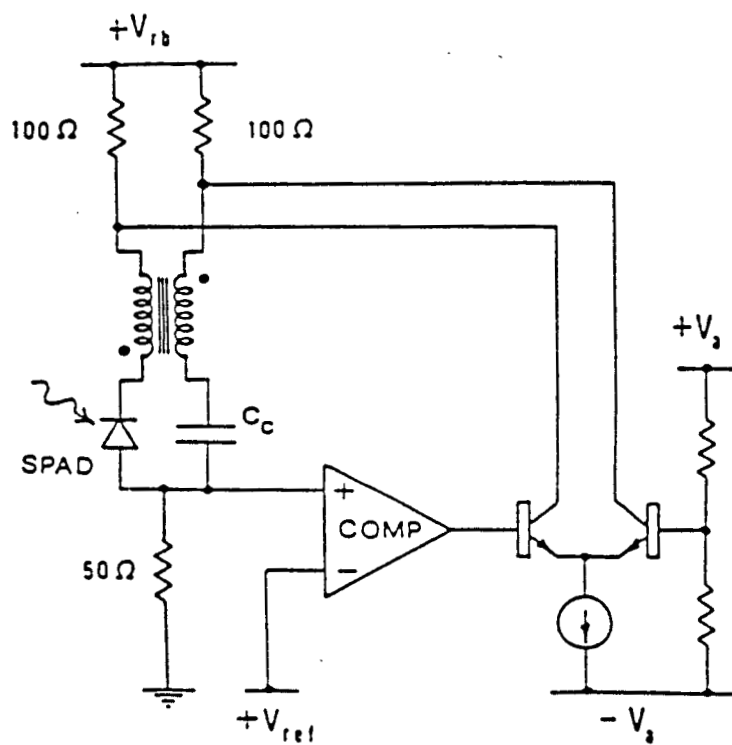
Figure 4.1. Simplified circuit used for active-quenching photon-counting operation of an APD [16].

17

As stated at the beginning of this chapter, the technique of multiple correlations relieves the requirement of a high signal-to-noise ratio; therefore, the true measure of performance is now the mean-square error of the time delay, which will be covered in the next chapter.

Table 4.1

Avalanche Photodiodes

Manufacturer	Model	Quantum Efficiency	Typical Gain	Capacitance(pF)
RCA	30902E	77%	150	1.6
RCA	30902S	77%	250	1.6
Fujitsu	FPD08	78%	<100	1.5
Hamamatsu	S2381	70%	100	2.0

CHAPTER 5. RANGING SYSTEM PARAMETERS

Besides the emitter and detector components, several other ranging system parameters must be evaluated. The expected number of signal counts per pulse is determined by developing a link equation, which includes the losses that the signal encounters while traveling to the target and back. The background noise is another derived parameter dependent on system conditions (i.e., sunlight, receiver aperture). The extinction ratio depends on the laser threshold energy, and then, the effects of time-resolved speckle fluctuations within the received pulses are determined by the type of target used in the ranging system.

Once these system parameters have been established, they are used in a qualitative measure of the system performance. The RMS error of the estimate of the range propagation time will later be shown to be the most applicable method for determining the proposed ranging technique's capabilities.

5.1 Ranging System Equations

The link equation for an optical system is developed much like one for an RF communications link. For the proposed ranging system, the optical transmitter consists of a modulator, either a laser diode or a laser diode array, and a beam expander/telescope. The receiver includes a telescope, an avalanche photodiode, and an amplifier. The telescopes act like antennas in an RF link. The received signal is then processed with the delayed version of the originally transmitted signal.

The received signal, disregarding noise, has encountered several phases of either attenuation or amplification. First, the efficiency of the transmitter and the gain of the transmitting telescope must be included in the link equation. Then the atmosphere attenuates the signal, the target usually provides some gain, and beam divergence causes some energy loss. The receiver also has a gain associated with the telescope and a detection system efficiency. Therefore, the expected counts per pulse for a cube-corner reflector target is calculated from [17]

$$<N> = \frac{\eta \, Q_T \, G \, T_a^2 \, A_R}{h\nu \, z^2} \, , \qquad (18)$$

where η = detector quantum efficiency,

$h\nu$ = energy of a photon,

z = range distance,

A_R = receiver area,

19

T_a^2 = two-way atmosphere transmittance,

Q_T = transmitted energy (transmitter gain and efficiency included),

G = target gain.

The transmitted energy and target gain can further be described by [17]

$$Q_T = \int d^2\rho \ |a(\rho,z)|^2 \int_{-\infty}^{\infty} dt \, |f(t)|^2 , \tag{19}$$

and

$$G = \sum_{m=1}^{M} \sigma_m \ |a(\rho_m,z)|^2 \ / \ \int d^2\rho \ |a(\rho,z)|^2 , \tag{20}$$

where ρ = horizontal coordinate vector on target surface measured from laser footprint's center,

$a(\rho,z)$ = complex amplitude cross-section of the laser footprint,

σ_m = lidar cross section of mth CCR,

$|f(t)|^2$ = transmitted laser pulse intensity,

M = number of CCRs illuminated by incident beam.

Assuming a Gaussian cross section for the laser footprint, Eq. (18) can now be written

$$<N> = \frac{\eta \ Q_T \, T_a^2 A_R \ \sum_{m=1}^{M} \sigma_m}{h\nu \ 2\pi \ z^4 \tan^2\theta_T} , \tag{21}$$

with θ_T = laser divergence angle. This analysis begins by examining a single point target; therefore, M=1. The lidar cross section is determined from

$$\sigma = \frac{\beta_r A_f^2}{\lambda^2} , \tag{22}$$

where β_r = target reflectivity,

A_f = effective area of the cube corner reflector,

λ = laser optical wavelength.

This system link equation, Eq. (21), predicts the average number of signal counts at the receiver. Now the expected background noise must be determined.

Background noise is dominated by the sun when it is present, but the stars, moon and man-made sources can also be important. Background noise enters the receiver either directly or indirectly from scattering and reflections. When the background noise source completely illuminates

the receiver field-of-view, its contribution to the detected power is determined by

$$P_b = N(\lambda) \, \Delta\lambda \, A_R \, \Omega_{FOV} \; . \qquad\qquad (23)$$

Here, Ω_{FOV} is the receiver's solid-angle field-of-view, $\Delta\lambda$ is the receiver's optical bandwidth, and

$N(\lambda)$ is the spectral radiance of the sources. Values for the spectral radiance are often approximated by blackbody radiation curves [18]. Figure 5.1 shows the diffuse component (the zenith angle of the sun is 45°) of the spectral radiance of a clear, day-time sky. Night-time noise is much less and usually contributes only a few photons. Blackbody radiation curves due to night objects can be found in Kopeika and Bordogna, 1970 [19]. The curves in Figure 5.1 are used later to derive typical values for background noise, although direct illumination from the sun would, of course, cause the worst case. Direct illumination, however, could possibly damage the detector sensitivity. Furthermore, for diffused sunlight or night operations, background noise is eventually found not be the dominating source of noise in this system.

The extinction ratio (laser "on" pulse transmitted energy/"off" pulse transmitted energy) is specific to the laser used. When it is included, the transmitted signal will consist of the original on-off pulses with a constant bias. The effects of the extinction ratio will be addressed later in the chapter.

Several types of targets can be used in laser ranging. Target reflectivity, shape and size are a few of the factors that determine the shape and strength of the laser pulse at the detector. Targets composed of cube-corner reflectors (CCRs) redirect the laser beam back upon the incident path, and since each CCR has a small area and is highly reflective, the pulse is minimally smeared and attenuated. Cube-corner reflectors actually provide gain at the target. If the target surface is rough on the optical scale, however, then it can reflect the beam in many directions, causing small-scale fluctuations, called speckle, in the signal energy detected at the receiver. A flat target causes the laser pulse to spread out , and depending on the range distance, can cause overlapping pulses in a continuously modulated system. Clearly, cube-corner reflectors are the best target surfaces because of their high gain. Calculations done in this paper that do not include speckle were made for a target of a single cube-corner reflector.

Fully developed speckle causes the laser footprint at the detector to be filled with a multitude of unordered bright and dark spots. This has little effect on the overall energy detected. A lesser developed degree of speckle could cause false intensity readings if the spots' areas are comparable to the area of the detector. It will be assumed that the target and ranging system allow for fully developed speckle. Because of the continuous signal pulses, it will be necessary to limit the range spread to a small portion of the pulse width. A range spread making the pulse larger than the chip width would cause intersymbol interference.
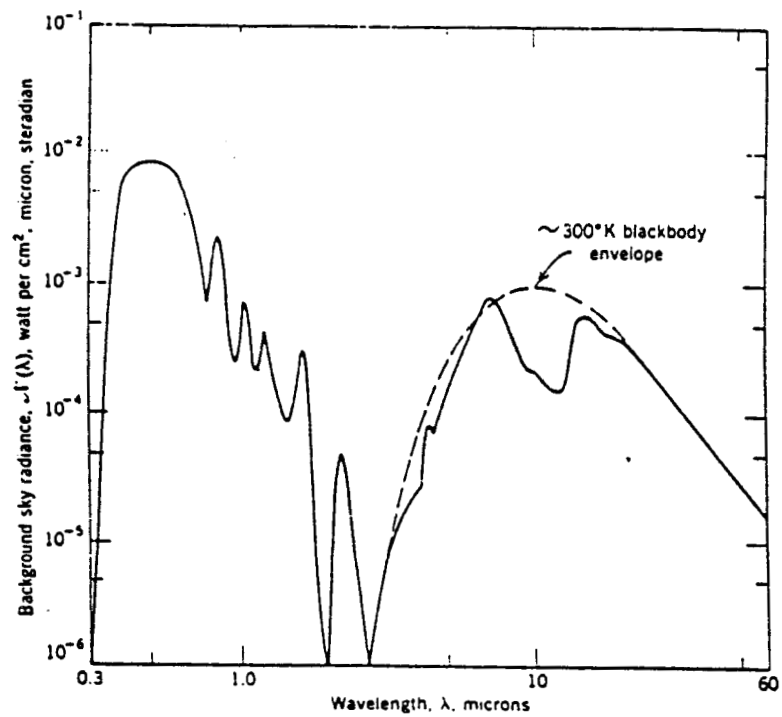
21

Figure 5.1. Measured spectral radiance of a clear, day-time sky. Taken at sea level.

5.2 The Maximum Likelihood Estimate of the Time Delay and Its Error

The maximum likelihood estimate of the time delay is the value of the delay, τ, which maximizes the count obtained by correlating the detected signal with a τ delayed version of the code. Since many sources of noise contribute to the detected signal, several maxima may exist after correlation. System performance is thus based on the probability of choosing the correct maxima, plus the error introduced by estimating the true delay.

The first derivation of the mean-square error given will include the detection process noises: background, thermal, shot and dark current. Next, the extinction ratio and speckle effects will each be introduced in the derivation to allow for clarity and comparisons of their impact on the result. Also, an ideal detector will continue to be used.

Starting with the assumption that the maximum count selected is indeed in the correct neighborhood, the variance, or error, of the estimate τ is found by taking the first two derivatives of the correlation function about the true delay τ_d (providing they exist). The derivative of the correlation function, $R(\tau)$, is expressed as

$$R(\tau) = R(\tau_d) + (\tau - \tau_d)R(\tau_d) + \dots \text{H.O.T,} \tag{24}$$

when Taylor series expansion around τ_d is performed. As τ is the point of maximum correlation, $R(\tau) = 0.0$ and Eq. (24) leads to

$$\varepsilon = (\tau - \tau_d) = -\frac{R(\tau_d)}{R(\tau_d)} \ . \tag{25}$$

The mean of the numerator is zero, and as long as $E\{R(\tau_d)\}^2 \gg \text{VAR}\{R(\tau_d)\}$, then the mean-square error can be written as [20]

$$\text{MSE} = \frac{E\{R^2(\tau_d)\}}{E^2\{R(\tau_d)\}} \ . \tag{26}$$

Referring back to the general ranging receiver diagram in Figure 2.2, it is apparent that

23

$$R(\tau_d) = \int_0^T s(t)\, a(t - \tau_d)\, dt \qquad (27)$$

Applying Eq. (27) to Eq. (26) results in the following equation for MSE:

$$MSE = \frac{\int_0^T \int_0^T <s(t_1)\, s(t_2)>\, a(t_1 - \tau_d)\, a(t_2 - \tau_d)\, dt_1\, dt_2}{\left[\int_0^T <s(t)>\, a(t - \tau_d)\, dt \right]^2} \ . \qquad (28)$$

It can be shown that

$$\int_0^T <s(t_1)>\, a(t_1 - \tau_d)\, dt_1 \int_0^T <s(t_2)>\, a(t_2 - \tau_d)\, dt_2 = 0.0 \ . \qquad (29)$$

Equation (29) allows the covariance to be used in the numerator of Eq. (28). The covariance is readily found from Campbell's theorem, as the mean and variance were found in Chapter 3. For a deterministic signal, the covariance is written

$$cov_s(t_1,t_2) = e^2 <G^2> \lambda_s \int_{-\infty}^{\infty} a(\alpha)\, h(t_1 - \alpha)\, h(t_2 - \alpha)\, d\alpha$$

$$+ \Lambda_{noise} \int_{-\infty}^{\infty} h(t_1 - \alpha)\, h(t_2 - \alpha)\, d\alpha \ , \qquad (30)$$

where

$$\Lambda_{noise} = e^2 <G^2> [\lambda_b + \lambda_G] + e^2 \lambda_L + \frac{2\, k_B\, T^o}{R_L} \ . \qquad (31)$$

Evaluating Eq. (28) yields a more applicable expression for the mean-square error of the maximum likelihood estimate:

$$MSE = \frac{8\, F\, \sigma_f^2}{<N_s>_T\, 3\sqrt{3}} + \frac{\sigma_f^2 \sqrt{\pi}}{2<N_s>^2} \left(\begin{array}{c} F <N_b>_T + F <N_G>_T \\ + \dfrac{<N_L>_T}{<G>^2} + \dfrac{2\, k_B\, T^o\, T'}{e^2\, R_L <G>^2} \end{array} \right) , \qquad (32)$$

24

where F = Gain excess noise factor

$<N_s>_T$ = expected total number of counts received during correlation period due to signal,

$\sigma_f = T_c / 4$ = Gaussian pulse width,

T' = Correlation period,

$<N_b>_T$ = Total number of counts detected due to background,

$<N_G>_T$ = Total number of counts contributed by bulk generated dark current,

$<N_L>_T$ = Total number of counts contributed by surface leakage current.

To maintain accuracy, it is essential that the RMS error, the square root of the MSE, remain smaller than the chip width.

5.3 Analysis of System Performance

The analysis of the continuously modulated laser ranging system's performance relies on applying typical values to Eq. (32) above. The values used are listed in Table 5.1, and were determined from realistic device parameters and calculations mentioned earlier in the chapter.

First, a plot of normalized RMS error versus the signal count indicated that the thermal noise is going to be dominant. This was confirmed when variations of the other noise values proved to have little or no effect on the outcome. Reducing the temperature 100K - 200K , in an effort to relieve the influence of thermal noise, had little effect on the error. Figure 5.2 is a graph of the RMS error normalized to the chip width versus the signal count. One on the vertical axis is where the RMS error equals the chip width. Varying the signal count is actually a result of varying the correlation time from 0.1 second to 10 seconds. Range distances of both 6000 km (LAGEOS orbit) and 600 km are shown. It is evident that ranging to 6000 km has too much error (several orders of magnitude greater than the chip duration), unless correlation times are extended to unrealistic lengths. Therefore, the rest of the analysis will be performed for a 600 km range.

When the extinction ratio, m, is included, the signal becomes

$$
<s(t)> = \begin{cases} \lambda_s (1 - \frac{1}{m})\, a(t) \; + \; \lambda_s (\frac{1}{m}) \; + N_{rate} & \text{-- on --} \\[2em] \lambda_s (\frac{1}{m}) \; + \; N_{rate} & \text{-- off --} \end{cases} \qquad (33)
$$

The "off power" term was simply added to the noise arrival rates, and the signal rate was multiplied by the attenuation factor (1 - 1/m). Figure 5.3 shows a comparison of the error when there is no extinction ratio, and when the power off is one-half the on power. Any ratio greater than 5 or 10 can be neglected for this system.

Table 5.1

Typical Values for a Satellite Laser Ranging System

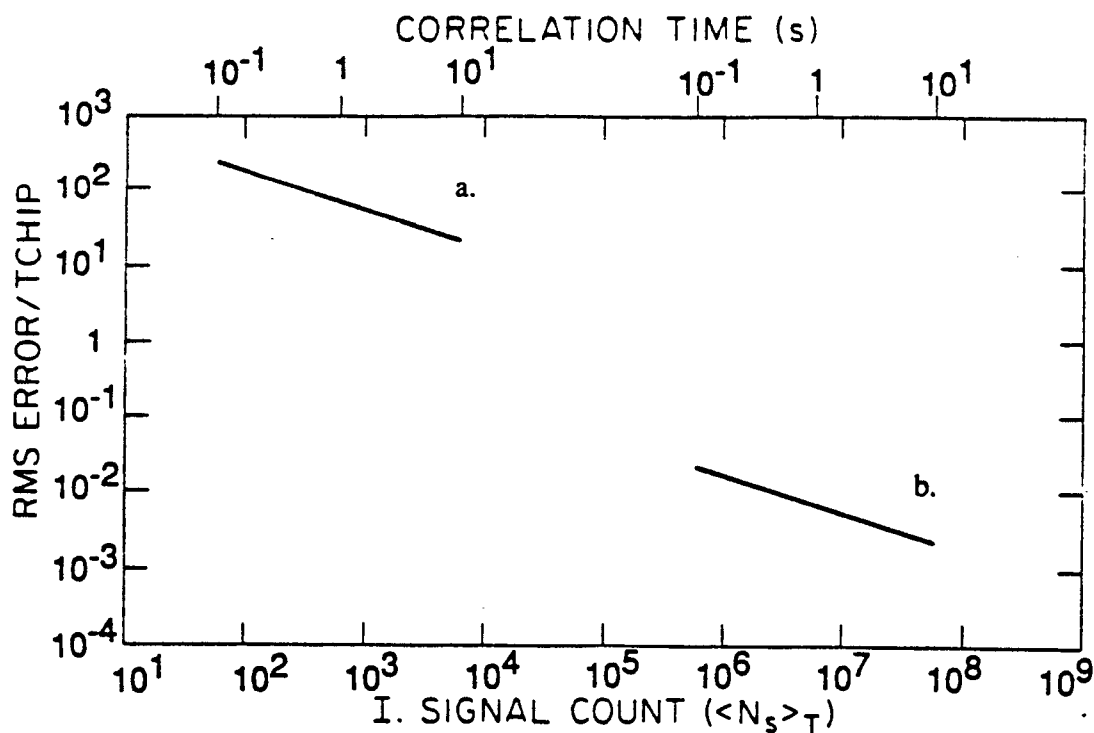|			
extinction ratio	= 10	background	= 5.0E5 counts/sec
bulk dark current	= 0.1 nA	temp	= 300K
surface current	= 10.0 nA	Rload	= 200 Ω
APD gain	= 250	T_c	= 1.0 ns
k_{eff}	= 0.02		

Figure 5.2. RMS error per chip vs. signal counts. Correlation time is from 0.1 to 10 seconds. Detection process noise only. a. Range = 6000 km b. Range = 600 km.
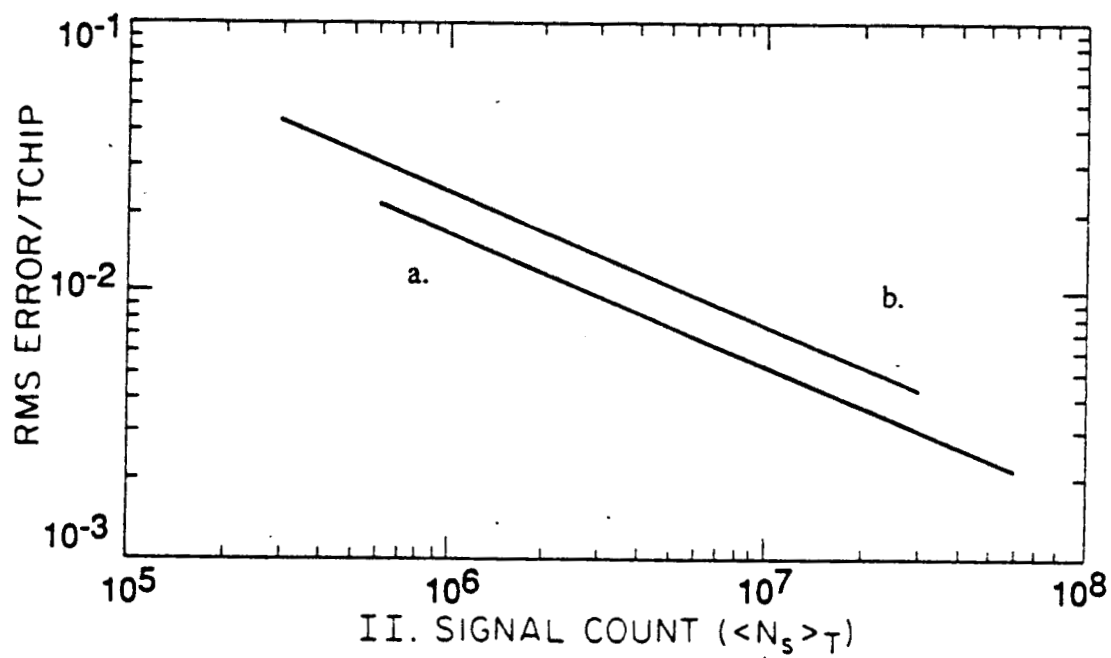
Figure 5.3. RMS error per chip vs. signal counts. Correlation time is from 0.1 to 10 seconds. a. Without extinction ratio   b. Extinction ratio = 2.

Adding speckle and range spread call for changing the target previously used, thus, a rederivation of the mean-square error. To begin with, the range spread, σ_T, is calculated as

$$\sigma_T = \frac{2\,z\,\tan\theta_T\,\tan\varphi}{c} \quad , \tag{34}$$

with φ as the beam incidence angle, θ_T the beam divergence angle, z the range distance and c the speed of light. Another parameter that will be needed is K, the ratio of receiver aperture area to the speckle correlation area. For diffuse, flat targets

$$K = \pi A_R \left(2 \tan\theta_T / \lambda \right)^2 \quad . \tag{35}$$

Now, range spread will be added to the detected signal pulse shape in the mean and covariance terms of the MSE Equation, (28). The delayed pulse shape will not have range spread. Since the pulse shapes are Gaussian, the mean and the covariance can now be written in counts per pulse as

$$\langle s(t)\rangle = \langle N_s\rangle_p\, G\!\left(\sqrt{\sigma_f^2 + \sigma_T^2}\,, t\right) \quad , \tag{36}$$

and

$$\text{cov}_s(t_1, t_2) = \langle N_s\rangle_p\, G\!\left(\sqrt{\sigma_f^2 + \sigma_T^2}\,, \frac{t_1 + t_2}{2}\right) \delta(t_1 - t_2)$$
$$+ \frac{\langle N_s\rangle_p^2}{K}\, G(\sqrt{2}\,\sigma_f\,, t_1 - t_2)\, G\!\left(\sqrt{\frac{\sigma_f^2}{2} + \sigma_T^2}\,, \frac{t_1 + t_2}{2}\right), \tag{37}$$

considering still the ideal detector, and with background noise added as in the previously developed mean and covariance equations.

Using the above now with Eq. (28), a new MSE is found:

$$\text{MSE} = \frac{F\,(\sigma_f^2 + \sigma_T^2)\,(2\sigma_f^2 + \sigma_T^2)^3}{\langle N_s\rangle_T\,\sigma_f^3\,(3\sigma_f^2 + 2\sigma_T^2)^{\frac{3}{2}}} + \frac{F\,\sigma_T^2\,(2\sigma_f^2 + \sigma_T^2)^3}{K\,8\,(\sigma_f^2 + \sigma_T^2)^{\frac{3}{2}}\,\sigma_f^3}$$
$$+ \frac{(\langle N_{ext}\rangle_T + \langle N_{noise}\rangle_T)\,\sqrt{\pi}\,(2\sigma_f^2 + \sigma_T^2)^3}{16\,\sigma_f^4\,\langle G\rangle^2\,\langle N_s\rangle_T^2} \quad . \tag{38}$$

A limit to the minimum mean-square error was found using this equation. As seen in Figure 5.4, a repeat of Figure 5.3 with Eq. (38), the speckle noise starts to dominate and causes the error to level off. So far, values for the 600 km range seem to be acceptable.

The effects of range spread and K are examined in Figures 5.5 and 5.6. In all cases range spread is considered to be less than the chip time. Unfortunately, evaluating Eq. (34), even at 600 km, yields a spreading of the pulse larger than the chip time. If the pulses spread larger than the chip time, then they will overlap, and intersymbol interference will occur. This violates one of the initial assumptions made at the beginning of the system evaluaton.

The PN code modulation satellite laser ranging technique already requires very tight parameters. Better target models may help the above evaluations absorb some of the error. With the typical values used, however, the ranging will be limited to less than 100 km.
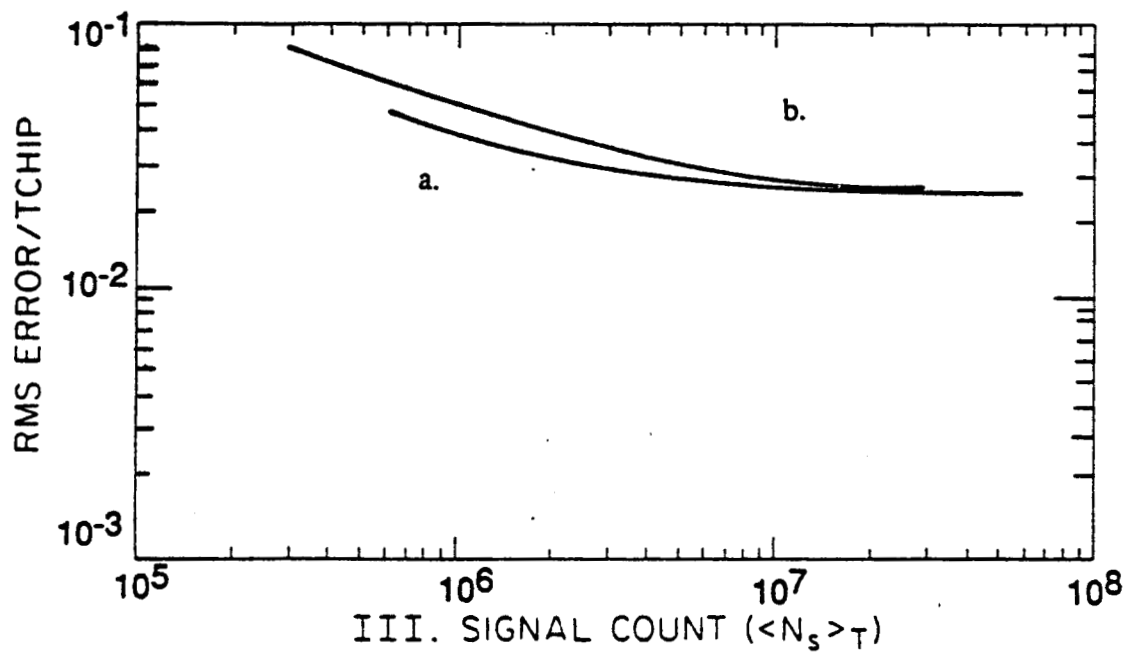
Figure 5.4. RMS error per chip vs. signal counts. Correlation time is from 0.1 to 10 seconds. Includes speckle. a. Without extinction ratio b. Extinction ratio = 2.
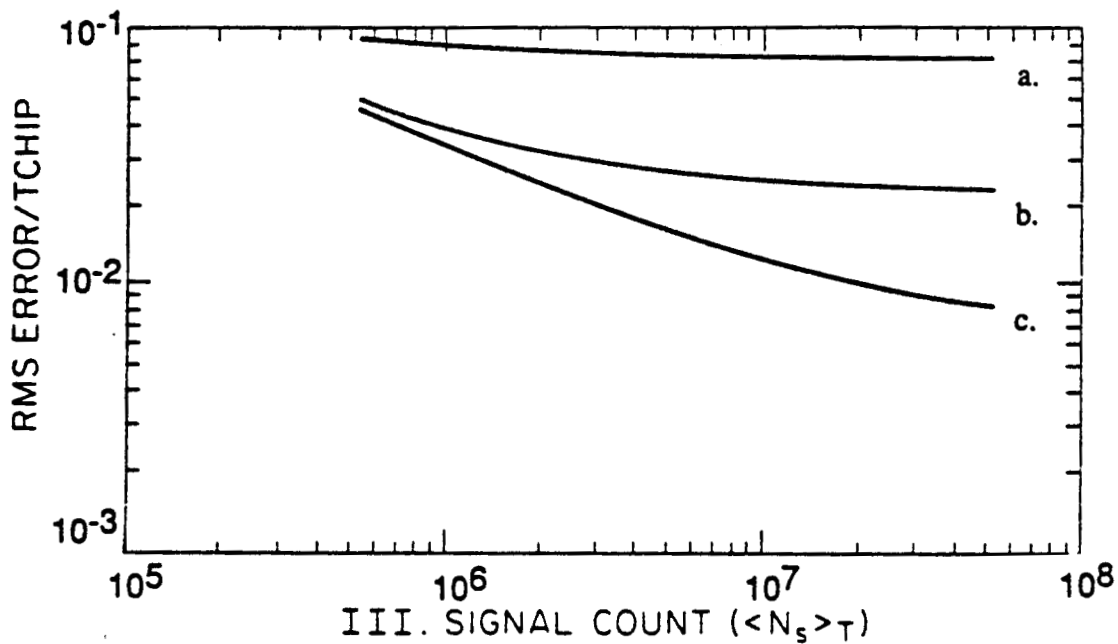
30

Figure 5.5.   RMS error per chip vs. signal counts. Correlation time is from 0.1 to 10 seconds. Includes speckle.   a. $K = 100$ b. $K = 1000$ c. $K = 10000$
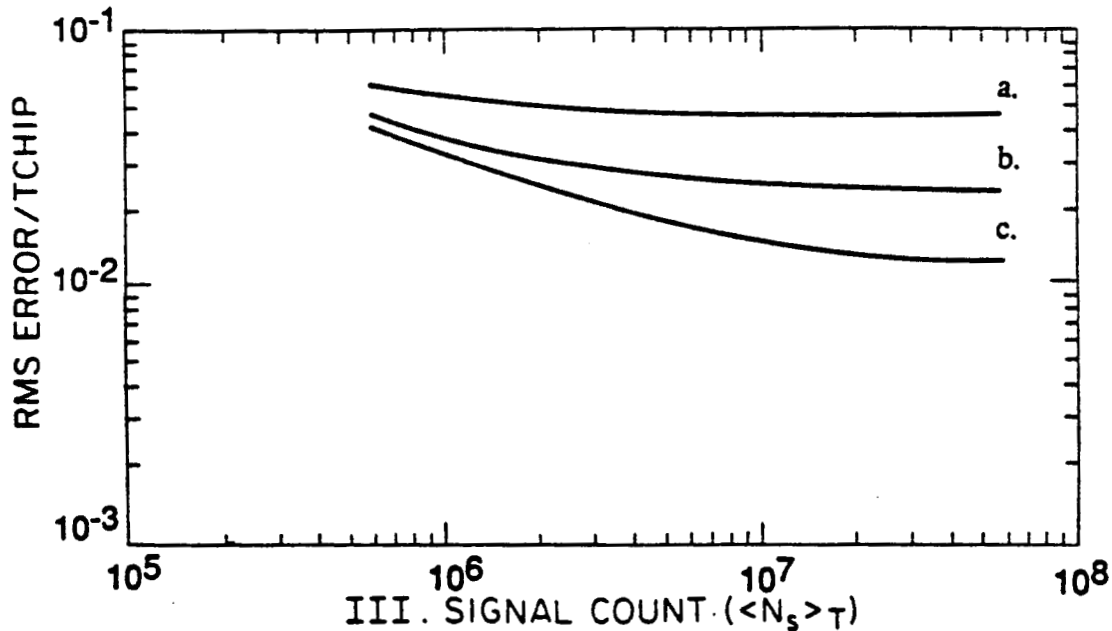

Figure 5.6.   RMS error per chip vs. signal counts. Correlation time is from 0.1 to 10 seconds. Includes speckle.   a. $\sigma_T = 2\sigma_f$ b. $\sigma_T = \sigma_f$ c. $\sigma_T = 0.5\sigma_f$

31

CHAPTER 6. CONCLUSIONS

For a ranging system that includes laser diodes and avalanche photodiodes, many sources of error must be considered, especially when the return signal is extremely low. Noise due to laser threshold, background radiation, dark current in the detector, thermal noise in the detector, and target-related speckle were all accounted for in this analysis. The effects of all but thermal noise and speckle were found to be negligible for reasonable values of system parameters.

When a satellite laser ranging system that operates on a continuously modulated PN code uses a flat, diffuse target, it is severely limited in range. A range greater than 100 km will cause intersymbol interference, adding more than an acceptable error to the system. For the ideal target of a single cube-corner reflector, a range of about 600 km yields enough signal to maintain a practical correlation time and achieve an RMS error less than the width of a code chip. If the range delay were acceptable, speckle noise would limit the minimum RMS error obtained, thus also limiting the required correlation time.

Several solutions to the ranging limitations are available. A better model for the target might result in better return signal strength and condition. An array of cube-corner reflectors is a possible target and is actually the goal of this ranging technique, but it is very difficult to model. Since the thermal noise contributes so much to the error of performance, a method of reducing it was sought. Applying cooler temperatures at the detector still did not alleviate its part in the RMS error. Increasing the correlation time is always a way to increase the signal count strength; however, it is limited by reasonable values.

Laser diodes are just now achieving the continuous wave output power used to model this ranging technique while maintaining beam quality. Further study into other error sources and target models is being made in order to fully analyze this ranging technique's capabilities.

REFERENCES

[1] J. J. Degnan, "Satellite laser ranging: current status and future prospects," IEEE Trans. Geosci. Remote Sensing, vol. GE-23, no. 4, pp. 398-413, July 1985.

[2] N. Takeuchi, H. Baba, K. Sakurai, and T. Ueno, "Diode-laser random-modulation cw lidar," Appl. Opt., vol. 25, no. 1, pp. 63-67, January 1986.

[3] R. M. Gagliardi and S. Karp, Optical Communications. New York: John Wiley & Sons, Inc., 1975.

[4] D. Botez, "Laser diodes are power-packed," IEEE Spectrum, vol. 22, no. 6, pp. 43-53, June 1985.

[5] M. Katzman, Ed., Laser Satellite Communications. New Jersey: Prentice-Hall, 1987.

[6] L. M. Holmes, "Commercial diode lasers break through 1-W level," Laser Focus, vol. 23, no. 4, pp. 74-78, April 1987.

[7] D. R. Scrifres, C. Lindstrom, R. D. Burnham, W. Streifer, and T. L. Paoli, "Phased-locked (GaAl)As laser diode emitting 2.6W from a single mirror," Electron. Lett., vol. 19, no. 5, pp. 169-171, March 3, 1983.

[8] R. L. Thorton, D. F. Welch, R. D. Burnham, T. L. Paoli and P. S. Cross, "High power (2.1 W) 10-stripe AlGa As laser arrays with Si disordered facet windows," Appl. Phys. Lett., vol. 49, no. 23, pp. 1572-1574, December 8, 1986.

[9] B. H. Candy, "Photomultiplier characteristics and practice relevant to photon counting," Rev. Sci. Instrum., vol. 56, no. 2, pp. 183-193, February 1985.

[10] B. L. Kasper, J. C. Campbell, J. R. Talman and A. H. Gnauck, "An 8-Gb/s optical receiver using an InGaAs avalanche photodiode and a GaAs preamplifiers," in Dig. Conf. on Lasers and Electro-Optics, Baltimore, MD April 26-May 1, 1987.

[11] J. Gowar, Optical Communication Systems. London: Prentice-Hall, 1984, pp. 375,389.

[12] R. J. McIntyre, "The distribution of gains in uniformly multiplying avalanche photodiodes: Theory," IEEE Trans. Electron Devices, vol. ED-19, no. 6, pp.703-712, June 1972.

[13] J. Conradi, "The distribution of gains in uniformly multiplying avalanche photodiodes: Experimental," IEEE Trans. Electron Devices, vol. ED-19, no. 6, pp. 713-718, June 1972.

[14] D. P. Schinke, R. G. Smith and A. R. Hartman, "Photodetectors," in Semiconductor Devices For Optical Communication (Topics in Applied Physics, vol. 39). H. Kressel, Ed., Berlin, Heidelberg, New York: Springer-Verlag, 1982.

[15] C. C. Chen and C. S. Gardner, "Comparison of direct and heterodyne detection optical intersatellite communication links," Electro-Optic Systems Lab., Univ. of Illinois, Urbana, IL, Rep. EOSL 87-002, March 1987.

[16]   S. Cova, A. Longoni and A. Andreoni, "Towards picosecond resolution with single-photon avalanche diodes," Rev. Sci. Instrum., vol. 52, no. 3, March 1981.

[17]   K.E. Im and C. S. Gardner, "Theoretical and experimental analyses of the performance of two-color laser ranging systems," Electro-Optic Systems Lab., Univ. of Illinois, Urbana, IL, Rep. EOSL 85-006, August 1985.

[18]   W. K. Pratt, Laser Communications Systems. New York: John Wiley & Sons, Inc., 1968.

[19]   N. Kopeika and J. Bordogna, "Background noise in optical communications systems," Proc. IEEE, vol. 58, no. 10, pp. 1571-1577, October 1970.

[20]   I. Bar-David, "Communication under the Poisson regime," IEEE Trans. Inf. Theory, vol. IT-15, no. 1, pp. 31-37, January 1969.

CUMULATIVE LIST OF RADIO RESEARCH LABORTORY

AND ELECTRO-OPTIC SYSTEMS LABORTORY REPORTS

PREPARED UNDER NASA GRANT NSG-5049

RRL Rep. No. 469 - Gardner, C. S. and N. N. Rao (December 1975),
     The Effects of Random Path Fluctuations on the Accuracy of
     Laser Ranging Systems.

RRL Rep. No. 471 - Zanter, D. L., C. S. Gardner and N. N. Rao
     (January 1976), The Effects of Atmospheric Refraction on
     The Accuracy of Laser Ranging Systems.

RRL Rep. No. 477 - Gardner, C. S. and J. R. Rowlett (November
     1976), Atmospheric Refraction Errors in Laser Ranging Data.

RRL Rep. No. 478 - Hendrickson, B. E. and C. S. Gardner
     (December 1976), Correction of Laser Ranging Data for
     the Effects of Horizontal Refractivity Gradients.

RRL Rep. No. 481 - Gardner, C. S. (February 1977), Statistics
     of the Residual Refraction Errors in Laser Ranging Data.

RRL Rep. No. 486 - Gardner, C. S. (July 1977), Comparison
     Between the Refraction Error Covariance Model and Ray
     Tracing.

RRL Rep. No. 488 - Gardner, C. S. (September 1977), Speckle
     Noise in Satellite Based Lidar Systems.

RRL Rep. No. 495 - Gardner, C. S. and G. S. Mecherle (April
     1978), Speckle Noise in Direct-Detection Lidar Systems.

RRL Rep. No. 496 - Gardner, C. S. and A. M. Saleh (October
     1978), Speckle Noise in Differential Absorption Lidar
     Systems.

RRL Rep. No. 499 - Gardner, C. S. (January 1979), A Technique
     for Remotely Measuring Surface Pressure from a Satellite
     Using a Multicolor Laser Ranging System.

RRL Rep. No. 502 - Palluch, E., J. D. Shelton and C. S. Gardner
     (May 1979), Operating Manual for the RRL 8 Channel Data
     Logger.

RRL Rep. No. 505 - Gardner, C. S. and R. Axford, Jr. (March
     1980), Regression Models for Multicolor Satellite Laser
     Ranging.

35

RRL Rep. No. 510 – Gardner, C. S. (April 1981), Analysis of
    Target Signatures for Laser Altimeters.

RRL Rep. No. 511 – Gardner, C. S. (June 1981), Atmospheric
    Refraction Effects in Air Borne Laser Ranging.

RRL Rep. No. 514 – Tsai, B. and C. S. Gardner (December 1981),
    Remote Sensing of Sea State by Laser Altimeters.

RRL Rep. No. 518 – Gardner, C. S. (August 1982), Optical
    Communications.

RRL Rep. No. 519 – Im, K. E. and C. S. Gardner (September 1982),
    Atmospheric Effects on Baseline Error in Satellite Laser
    Ranging Systems.

RRL Rep. No. 526 – Im, K. E., B. M. Tsai and C. S. Gardner
    (September 1983), Analysis of Short Pulse Laser Altimetry
    Data Obtained over Horizontal Path.

RRL Rep. No. 527 – Tsai, B. M. and C. S. Gardner (March 1984),
    Theoretical and Experimental Analysis of Laser Altimeters
    for Barometric Measurements Over the Ocean.

EOSL Rep. No. 84-001 – Lafaw, D. A. and C. S. Gardner (August
    1984), Timing Performance of Phase-Locked Loops in Optical
    Pulse Position Modulation Communication Systems.

EOSL Rep. No. 85-002 – Im, K. E. and C. S. Gardner (April 1985),
    Estimation of the Differential Pulse Propagation Times in
    Two-Color Laser Ranging Systems.

EOSL Rep. No. 85-003 – Chen, C. C. and C. S. Gardner (May 1985),
    Phase-Locked Loop Synchronization for Direct Detection
    Optical PPM Communication Systems.

EOSL Rep. No. 85-006 – Im, K. E. and C. S. Gardner (August 1985),
    Theoretical and Experimental Analysis of the Performance
    of Two-Color Laser Ranging Systems.

EOSL Rep. No. 87-002 – Chen, C. C. and C. S. Gardner (March
    1987), Comparison of Direct and Heterodyne Detection Optical
    Intersatellite Communication Links.

EOSL Rep. No. 87-003 – Natarajan, S. and C. S. Gardner (May
    1987), Phase Error Statistics of a Phase-Locked Loop
    Synchronized Direct Detection Optical PPM Communication
    System.

EOSL Rep. No. 87-004 – G. Hugh Song and C. S. Gardner (June
    1987), Single-Color Laser Ranging with a Cube-Corner-
    Retroreflector Array.

36

EOSL Rep. No. 87-007 - Ball, C. K. (December 1987), Evaluation
of a Satellite Laser Ranging Technique Using Pseudonoise
Code Modulated Laser Diodes.

PAPERS PUBLISHED

C. S. Gardner, "Effects of Random Path Fluctuations on the
Accuracy of Laser Ranging Data," Applied Optics, 15,
2539-2545, October 1976.

C. S. Gardner, "Effects of Horizontal Refractivity Gradients on
the Accuracy of Laser Ranging to Satellites," Radio
Science, 11, 1037-1044, December 1976.

C. S. Gardner, "Correction of Laser Tracking Data for the Effects
of Horizontal Refractivity Gradients," Applied Optics, 16,
2427-2432, September 1977.

C. S. Gardner, R. Rowlett and B. E. Hendrickson, "Ray Tracing
Evaluation of a Technique for Correcting the Refraction
Errors in Satellite Tracking Data," Applied Optics, 17,
3143-3145, October 1978.

C. S. Gardner, "Technique for Remotely Measuring Surface Pressure
from a Satellite Using a Multicolor Laser Ranging System,"
Applied Optics, 18, 3184-3189, September 1979.

C. S. Gardner, "Target Signatures for Laser Altimeters: An
Analysis," Applied Optics, 21, 448-453, February 1982.

B. M. Tsai and C. S. Gardner, "Remote Sensing of Sea State Using
Laser Altimeters," Applied Optics, 21, 3932-3940, November
1982.

C. S. Gardner, B. M. Tsai and J. B. Abshire, "Remote Sensing of
Atmospheric Pressure and Sea State from Satellites Using
Short-Pulse Multicolor Laser Altimeters," Proceedings of
NATO-AGARD Symposium on Propagation Factors Affecting
Remote Sensing by Radio Waves, 345, (46-1)-(46-11),
Oberammergau, FRG, May 24-28, 1983.

C. S. Gardner, B. M. Tsai and K. E. Im, "Multicolor Laser
Altimeters for Barometric Measurements over the Ocean:
Theoretical," Applied Optics, 22, 2571-2577, September 1,
1983.

37

C. S. Gardner and J. B. Abshire, "Atmospheric refraction and target speckle effects on the accuracy of laser ranging systems," Proc. Int. Conf. on Laser Ranging Instrumentation, 1, 29-41, Royal Greenwich Observatory, Hearstmonceux, UK, September 24-28, 1984 (invited paper).

B. M. Tsai and C. S. Gardner, "Time-Resolved Speckle Effects on the Estimation of Laser Pulse Arrival Times," J. Opt. Soc. Amer. A., 2, 649-656, May 1985.

J. B. Abshire and C. S. Gardner, "Atmospheric Refractivity Corrections for Satellite Laser Ranging," IEEE Trans. Geosci. Remote Sensing, GE-2, 414-425, July 1985.

C. S. Gardner, "Remote Sensing of Atmospheric Pressure and Sea State Using Laser Altimetry," Proc. 1985 Int. Geosci. Remote Sensing Symps., 1, 199-206, Amherst, MA, October 7-9, 1985.

K. E. Im and C. S. Gardner, "Estimation of Differential Pulse Propagation Times in Two-Color Laser Ranging Systems," J. Opt. Soc. Amer. A., 3, 143-156, Jan. 1986.

C. C. Chen and C. S. Gardner, "Performance of Phase Locked Loop Synchronized Optical PPM Communication Systems," IEEE Trans. Comm., COM-34, 988-994, Oct. 1986.

C. C. Chen and C. S. Gardner, "Loss Factors Associated with Spatial and Temporal Tracking Error in Intersatellite PPM Communication Links," Proc. IEEE Global Telescom Conf., 3, 1392-1397, Houston, TX, Dec. 1-4, 1986.

K. E. Im, C. S. Gardner, J. B. Abshire and J. F. McGarry, "Experimental evaluation of the performance of pulsed two-color laser ranging systems," J. Opt. Soc. Amer. A., 4, 820-833, May 1987.

C. C. Chen and C. S. Gardner, "Impact of Random Pointing and Tracking Errors on the Design of Coherent and Incoherent Optical Intersatellite Communication Links," IEEE Trans. Comm., to be published, 1987.

38